Optimization of a Cl_2-H_2 inductively coupled plasma etching process adapted to nonthermalized InP wafers for the realization of deep ridge heterostructures

S. Guilet and S. Bouchoule[a)]
Laboratoire de Photonique et de Nanostructures (LPN)—CNRS, Route de Nozay, 91460 Marcoussis, France

C. Jany
GIE Alcatel Thales III-V Lab, Route de Nozay, 91460 Marcoussis, France

C. S. Corr[b)] and P. Chabert
Laboratoire de Physique et Technologie des Plasmas (LPTP)—CNRS—Ecole Polytechnique, 91128 Palaiseau, France

(Received 16 June 2006; accepted 8 August 2006; published 25 September 2006)

Inductively coupled plasma etching using Cl_2-H_2 chemistry with no additive gas (CH_4, Ar, or N_2) is studied to realize deep (>5 μm) ridges with smooth and vertical sidewalls. The process is optimized for nonthermalized InP wafers to avoid the use of thermal grease. Cleaning of the rear side of the wafer after etching is avoided, which is suitable for an industrial process or for critical subsequent steps such as epitaxial regrowth. The influence of the Cl_2/H_2 ratio on the etching mechanism is investigated for both InP bulk layers and InGaAs/InP or InGaAlAs/InP heterostructures. The authors show that this ratio is the main parameter controlling the ridge profile, in a similar way for both bulk InP and InGa(Al)As/InP samples. Smooth and vertical sidewalls with neither undercuts nor notches can be obtained in the 0.5–1 mT pressure range for a hydrogen percentage of 35%–45% in the gas mixture. Etching rates from 900 to 1300 nm/min together with a selectivity over SiN_x dielectric mask as high as 24:1–29:1 are measured for the InP bulk layers under these conditions. Etching does not affect the optical quality of the heterostructures as evidenced from micro-photoluminescence measurements performed on 1.6- to 0.85-μm-wide deep etched ridge waveguides. The process is well adapted to the realization of low loss deep ridge waveguides or buried heterostructures. © *2006 American Vacuum Society.*
[DOI: 10.1116/1.2348728]

I. INTRODUCTION

Etching of high aspect ratio deep ridge InP-based heterostructures is a critical building block for photonic device fabrication. Deep ridge waveguides are indeed key elements to realize highly confined InP-based photonics circuits.[1,2] For this purpose, a dry-etching process that can produce narrow, single transverse mode, ridge waveguides with a highly anisotropic profile and smooth sidewalls free from undercuts or notches is required to minimize the optical scattering losses. Deep ridge waveguides are also needed to realize high-speed (>40 Gbits/s) active devices such as lasers or modulators based on buried heterostructures.[3] The waveguide is generally buried in semi-insulating InP (SI:InP) using a planarizing selective epitaxial regrowth. It was shown that a regrowth thickness of 5 μm or more is needed to obtain a capacitance value which is low enough to achieve a 40 GHz bandwidth.[3] A nearly perfect deep ridge profile presenting smooth sidewalls without any undercut nor lateral etching difference between the various materials is required in order to guarantee a smooth and defect free epitaxial regrowth.

Inductively coupled plasma (ICP) etching of high aspect ratio InP-based waveguides has been widely developed for such applications in the recent years, using Cl_2 as the main etching gas, and critical parameters have been pointed out. First, a high sample temperature is necessary to achieve smooth etching of InP due to the low volatility of the $InCl_x$ reaction products. In many studies the sample is thus glued to the sample carrier in order to control the thermal transfer from the heated electrode.[4–6] Second, additive gas has been introduced in order to obtain a vertical sidewall, since deep ridge etching with pure Cl_2 generally leads to severe undercuts.[2,7] $Cl_2/CH_4/H_2$ chemistry has been widely used to anisotropically etch InP-based heterostructures with both electron cyclotron resonance and ICP techniques,[7–10] using CH_4 to balance the removal of In and P elements and to introduce some polymer-induced sidewall passivation.[7,10] However, this chemistry is prone to polymer and amorphous carbon formations, and significant redeposition may occur on the whole sample surface. Cl_2/N_2 mixture has also been studied since sidewall passivation can be obtained for high N_2 concentration.[1,4,11–14] But the etching speed and the selectivity over dielectric mask are simultaneously significantly decreased in this case.[4,13,14] Finally, H_2 has been added to a standard Cl_2/Ar process,[2] and deep ridge etching of

[a)]Electronic mail: sophie.bouchoule@lpn.cnrs.fr
[b)]Present address: SP3, Plasma Research Laboratory, ANU, Canberra, Australia.

InP/InGaAsP heterostructures with smooth and vertical sidewalls has been demonstrated in a specific regime balancing the Cl_2-H_2 chemical etch and the Ar physical component, with all the epitaxial layers being etched at approximately the same rate.

In this article, we investigate the use of Cl_2-H_2 chemistry with no additive gas to etch deep (>5 μm) InGa(Al)As/InP heterostructures with smooth and vertical sidewalls. The process is adapted to the etching of nonthermalized InP wafers in order to avoid the use of thermal grease, which is convenient for an industrial process and/or for critical subsequent steps such as epitaxial regrowth. The Cl_2/H_2 ratio is evidenced as the main parameter controlling the etching mechanism and the ridge sidewall profile, and a similar etching behavior occurs for both bulk InP layers and InGa(Al)As/InP heterostructures. Smooth and vertical sidewalls with no undercuts can be obtained in the 0.5–1 mT pressure range, with almost no difference in lateral etching between the InP and the InGa(Al)As layers, despite a significant difference in the planar etching rate of these materials. The InP etching rates are 900–1300 nm/min in this pressure range, and high selectivities over a SiN_x dielectric mask of 24:1–29:1 are obtained, presumably due to the reduced physical etching component with this gas mixture. This high selectivity is an important point for the subsequent selective epitaxial regrowth step, using the remaining dielectric layer as the regrowth mask. An aspect ratio of 10 to 13 (for 0.5-μm-wide patterns) is measured for bulk InP layers and InGa(Al)As/InP periodic heterostructures, respectively.

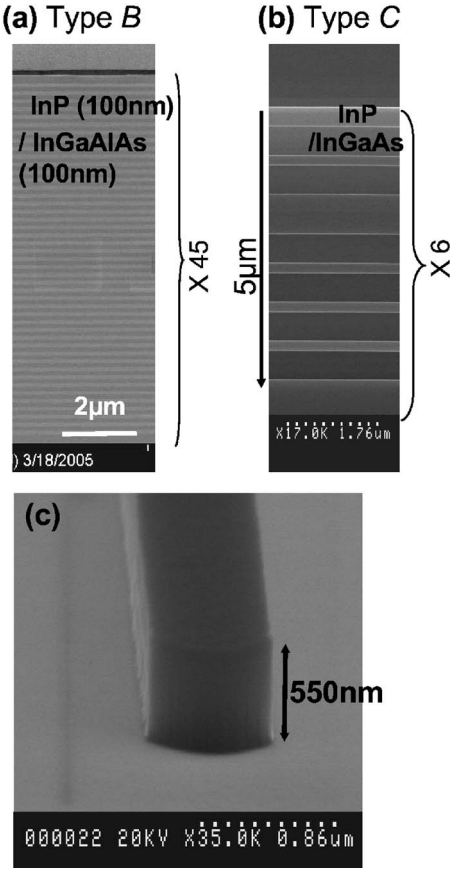

FIG. 1. Cross-section SEM images of the (a) type-*B* and (b) type-*C* structures. (c) SEM image of the dielectric mask.

II. GENERAL ETCHING CONDITIONS

A. Experimental conditions

The samples were etched in a Sentech SI-500 planar triple spiral antenna ICP etch system. The reactor chamber is made of anodized aluminum. The ICP source (rf of 13.56 MHz) is coupled to the plasma through an Al_2O_3 ceramic window. The sample is deposited on a 4 in. carrier transferred to the reactor chamber via a loadlock, and mechanically clamped above the rf (13.56 MHz) biased electrode with an Al_2O_3 ceramic clamping ring. The electrode temperature is controlled during etching by a combination of water cooling at a fixed temperature and regulated resistive heating. The sample carrier is thermally coupled to the electrode with He backside cooling. Samples are either glued to the carrier using heat conducting vacuum grease (thermalized sample) or left thermally decoupled from the carrier (nonthermalized sample). In the first case, the sample temperature can be considered as mainly controlled by the electrode and not driven by plasma heating. In the latter case, He backside cooling is still switched on, but no grease is used to attach the sample. The nonthermalized samples may thus be considered as thermally isolated from the electrode and the temperature of the sample surface mainly imposed by the plasma conditions.

The etched structures were either bulk *n*-doped InP substrates (type *A*) or test heterostructures consisting of a periodic stack of InGaAlAs (27% Al)/InP (type *B*) and InGaAs/InP layers (type *C*) in order to study the influence of the material composition on the deep ridge etching performance. Cross-section scanning electron microscope (SEM) images of the type-*B* and type-*C* structures are reported in Figs. 1(a) and 1(b). All wafers were patterned with 4-, 1.7-, 0.85-, and 0.6-μm-wide, and 500-nm-thick SiN_x stripes, defined by UV-300 lithography and subsequent CHF_3/O_2 reactive ion etching. A dielectric mask with reproducible vertical sidewalls was obtained with this process [see Fig. 1(c)], which is a critical point to avoid lateral sidewall erosion of the deep ridge during ICP etching, as reported in Ref. 15, and to obtain reproducible results. The mask definition is obviously limited by the UV lithography technique, as evidenced in Fig. 1(c) by the striations transferred from the positive photoresist to the sidewall of the dielectric mask, as well as by other imperfections in the optical mask.

The wafers were then cleaved into 7×7 mm^2 samples for the study. A preliminary process optimization was performed on InP samples with a silicon carrier, a H_2 percentage in the gas mixture fixed to 30%, and an ICP power of 500 W. These two latter values actually correspond to intermediate values within the process window, as will be shown in Secs. II C and III. It was found that a substrate temperature higher than 150 °C and an electrode rf power higher than 90 W

(corresponding to a dc bias higher than −120 V) were necessary to smoothen the etched surface of the thermalized samples.

No significant modification of the ridge sidewall profile was observed in the 0.5–1 mT pressure range when increasing the dc bias amplitude from −120 to −200 V. The dc bias was thus fixed to a value of −145 V, corresponding to a good compromise between the etching rate and the selectivity over the SiN_x mask. The electrode temperature was fixed to 190 °C to ensure a smooth etched surface.

The pressure was restricted to less than 2 mT since higher working pressure values were found to enhance the ridge sidewall roughness and the etching isotropy. In the 0.5–1 mT pressure range, changing the total flow rate between the minimum value of ~10 standard cubic centimeter per minute (sccm) (limited by the mass flow controller resolution) and the maximum value of 28 sccm (limited by the pumping system at 0.5 mT) did not influence the etching rate nor the etching isotropy significantly. This was in contrast with the high pressure range (typically above 2 mT) where the etching rate could be strongly increased by increasing the flow rate while keeping the InP etched surface very smooth. An etching rate as high as 4 μm/min could be achieved at 5 mT with a total flow rate of 200 sccm. However, the ridge sidewall was always rougher in the high pressure range, which is unsuitable for deep ridge etching. The total flow rate was thus fixed to either 14 or 28 sccm in the following experiments, both values leading to similar etching results.

B. Influence of carrier material

Several carrier materials were tested including silicon, pure aluminum, and quartz. We found that for the same plasma conditions the wafer carrier material has a dramatic effect on the surface roughness of the etched InP samples. The detailed study is beyond the scope of this article, but the aluminum carrier always led to rougher etched surfaces. This effect is illustrated for both thermalized and nonthermalized samples in Figs. 2(a)–2(d), comparing the etching results obtained for fixed plasma conditions (T=190 °C, 1 mT, 500 W ICP power, −145 V dc bias, and H_2 percentage of 30%) with the silicon and the aluminum carriers. The roughness is particularly increased in the case of thermalized InP samples. Since both carriers have a similar thickness of 500 μm, and since the thermal conductivity κ and thermal diffusivity D of aluminum and silicon are also very similar (κ ~230 W m^{-1} K^{-1} and 150 W m^{-1} K^{-1}, and D~0.950 and 0.900 cm^2 s^{-1} at 300 K for aluminum and silicon, respectively), it can be expected that the same temperature is achieved in both cases at the surface of the thermalized samples for a fixed electrode temperature. Consequently, the roughness difference cannot be explained by a significant variation of the sample temperature. Our results suggest that the reaction products of silicon in the Cl_2-H_2 chemistry significantly contribute to the etching of the InP samples. This is consistent with similar observations reported with pure Cl_2 chemistry.[16]

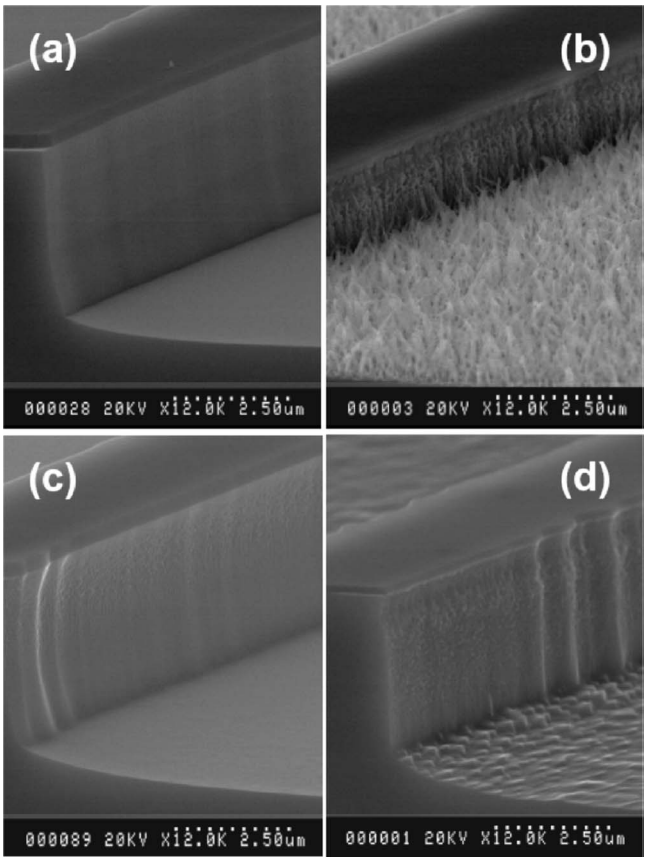

FIG. 2. SEM images of [(a) and (b)] thermalized and [(c) and (d)] nonthermalized InP samples etched for 5 min with T=190 °C, 1 mT, 500 W ICP power, −145 V dc bias, and Cl_2/H_2=10/4 sccm. [(a) and (c)] Silicon carrier. [(b) and (d)] Aluminum carrier.

We furthermore evidenced that the carrier material also has a strong influence on the etching anisotropy. Figures 3 and 4 compare the ridge profile obtained for nonthermalized InP samples for fixed plasma conditions (T=190 °C, 0.5 mT, 800 W ICP power, and −145 V dc bias) using the silicon and the aluminum carriers. The H_2 percentage was set to ~30% and ~36% in Figs. 3 and 4, respectively. These values correspond to the anisotropic regime, as will be shown in Sec. III. A relatively smooth etched surface was

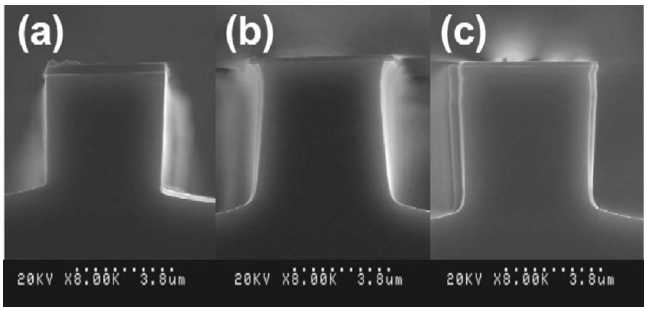

FIG. 3. Cross-section SEM images of nonthermalized InP samples etched for 7 min with T=190 °C, 0.5 mT, 800 W ICP power, −145 V dc bias, and Cl_2/H_2=20/8 sccm. (a) Silicon carrier. (b) Aluminum carrier. (c) Aluminum carrier with silicon pieces.

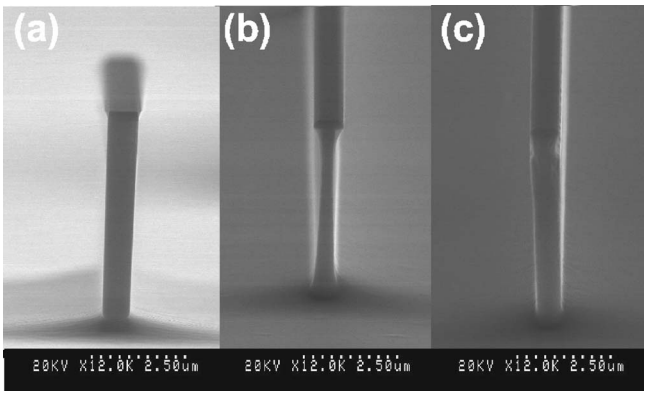

FIG. 4. SEM images of nonthermalized InP samples etched for 5 min with $T=190\,^{\circ}C$, 0.5 mT, 800 W ICP power, −145 V dc bias, and $Cl_2/H_2=18/10$ sccm. (a) Silicon carrier. (b) Aluminum carrier. (c) Aluminum carrier with silicon pieces.

obtained even with the aluminum carrier at this high ICP power. However, while highly anisotropic etching with almost vertical ridge sidewalls is obtained with the silicon carrier, the use of aluminum carrier led to isotropic etching with significant mask underetching. We observed that the etching anisotropy can be significantly enhanced by simply depositing pieces of silicon on the aluminum carrier around the InP sample. This effect is evidenced in Figs. 3(c) and 4(c). This experiment demonstrates that the silicon surface has a significant impact on the plasma chemistry and the InP etching process. The large amount of Si^+ or $SiCl_x^+$ species in the plasma evidenced in the spectroscopic studies of Ref. 17, and resulting from the etching of silicon by chlorine, can be involved in this beneficial effect. A silicon carrier is thus used for all the following experiments.

C. Influence of ICP power

Figure 5(a) shows the typical evolution of the etching rate as a function of ICP power for thermalized and nonthermalized bulk InP samples, and for a cathode temperature set to 190 °C. Other parameters are $P=1$ mT, fixed dc bias $V_b=-145$ V, and a moderate H_2/Cl_2 ratio of 4/10. As can be deduced from the figure, an ICP power of ~200 W or more was necessary to get a sufficient flux of ions impinging the surface and heating the nonthermalized sample to achieve a significant etching rate. This is consistent with electron density and ion current density measurements simultaneously performed with a compensated Langmuir probe and reported in Fig. 5(b), showing that the onset of the high density inductive mode occurs at ICP power above ~200 W in our system. The ridge profiles of thermalized and nonthermalized InP etched samples are reported in Figs. 6(a)–6(c) for ICP powers of 350, 500, and 800 W. One can notice that perfectly vertical sidewalls were never obtained with this moderate H_2/Cl_2 ratio under these etching conditions. Similar etching rates and sidewall profiles, were obtained for both thermalized and nonthermalized samples around 350 W, which indicates that similar temperatures should be reached at the sample surfaces. The etching rate of the nonthermalized sample is increased by further increasing the ICP power [Fig. 5(a)], allowing us to reduce the etching time; however, the sidewall profile tends to become more isotropic and becomes rapidly unsuitable.

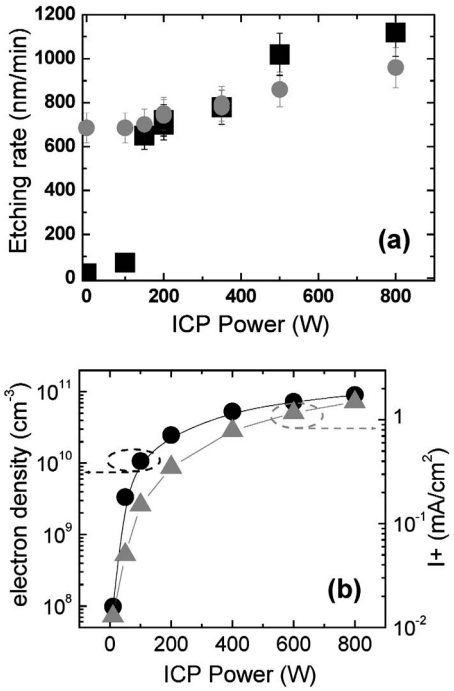

FIG. 5. (a) InP etching rate measured as a function of ICP power for thermalized (dots) and nonthermalized (squares) samples, with $T=190\,^{\circ}C$, 1 mT, 500 W ICP power, −145 V dc bias, and $Cl_2/H_2=10/4$ sccm. (b) Electron density (dots, left axis) and positive ion current density (triangles, right axis) measured as a function of ICP power under the same plasma conditions.

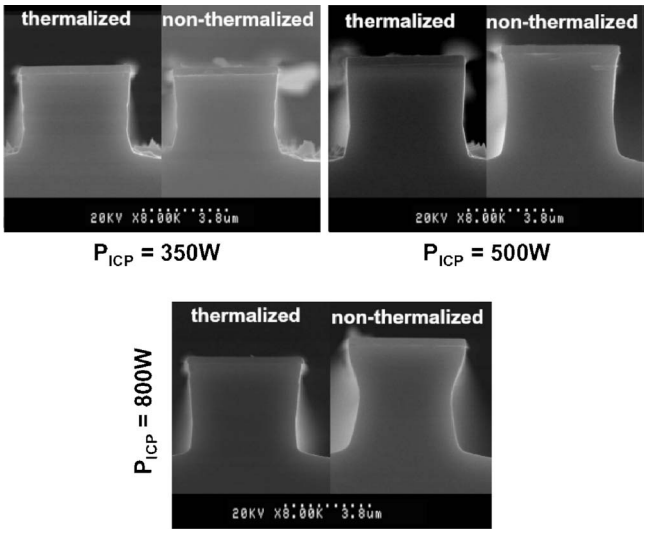

FIG. 6. Cross-section SEM images of thermalized (left) and nonthermalized (right) InP samples etched for $T=190\,^{\circ}C$, 1 mT, −145 V dc bias, $Cl_2/H_2=10/4$ sccm, and for ICP powers of 350, 500, and 800 W.

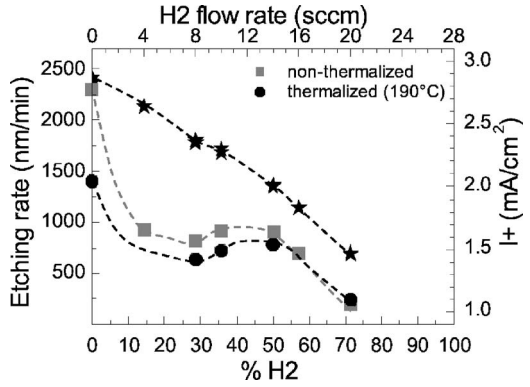

FIG. 7. Positive ion current density (right axis, stars) and etching rate (left axis) of nonthermalized (squares) and thermalized (dots) InP samples as a function of the H_2 percentage in the Cl_2-H_2 gas mixture. The other plasma conditions are $T=190$ °C, 0.5 mT, 800 W ICP power, −145 V dc bias, and total flow rate of 28 sccm.

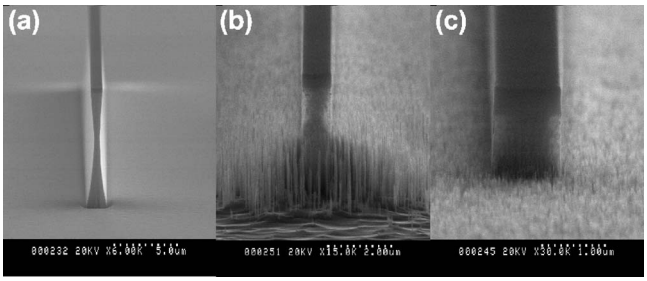

FIG. 8. SEM images of the InP samples etched for 5 min in the conditions of Fig. 7 for a H_2 percentage of (a) 0%, (b) 57%, and (c) 70%. The samples are nonthermalized.

III. PROCESS OPTIMIZATION

A. H_2 Influence on the etched profile

Optimizing the H_2/Cl_2 ratio allows us to obtain highly vertical sidewalls for the nonthermalized samples in the 0.5–1 mT pressure range, even for high ICP power and high etching rate. The etching rate of nonthermalized InP samples is reported in Fig. 7 as a function of H_2 percentage for an ICP power of 800 W and a working pressure of 0.5 mT. Other parameters are $T=190$ °C, fixed dc bias $V_b=-145$ V, and total flow rate of 28 sccm. The etching rate of the thermalized samples is also reported for comparison. Similar curves were obtained for $P=1$ mT.

The positive ion current density $I+$ was monitored during the etching using a rf planar probe installed at the reactor wall.[18] The variation of $I+$ with H_2 percentage is also reported in Fig. 7. $I+$ linearly decreases with the increase of H_2 percentage. The ion current is typically reduced by a factor of ~2 when the H_2 concentration is varied from 0% to 70%, which has to be related to the higher hydrogen dissociation energy.

For low hydrogen percentage (typically lower than 25%), a high etching rate and a smooth etched surface were obtained for both thermalized and nonthermalized samples. However, the ridge profile exhibited a strong undercutting of the mask, as illustrated in Fig. 8(a). On the other hand, at high hydrogen percentage (typically higher than 50%), the etched surface became extremely rough as illustrated in Figs. 8(b) and 8(c). This strong roughness is likely due to the preferential removal of P elements by hydrogen via the formation of PH_x reaction products, compared to the limited removal of In element by chlorine, when the H_2 flow dominates the Cl_2 flow.

As can be seen in Fig. 7, the etching rate is dramatically decreased at the same time. The strong reduction by a factor of ~10 cannot be explained by the moderate ion current density decrease by a factor of ~2. Moreover, since the same tendency is observed for both nonthermalized and thermalized (190 °C) samples, the etching rate reduction cannot be explained by a temperature decrease at the sample surface due to the reduction of the ion flux. We assume that the increase in H_2 concentration reduces the Cl radical density by formation of secondary products, such as HCl,[19] which in turn decreases the etching rate. This observed decrease constitutes a main difference with the Cl_2-Ar-H_2 chemistry, for which a significant etching rate increase is reported at high H_2 concentrations.[2]

Starting from the low H_2 concentration region, increasing the H_2/Cl_2 ratio allows us to obtain smooth structures with a high degree of anisotropy. Increasing the H_2 concentration first promotes the removal of P element and contribute to the balancing between P and In etching at elevated temperatures.[7] Second, it decreases the Cl radical density, which in turn reduces the chemical lateral etching component responsible for the sidewall underetching and the isotropic profile. This effect is illustrated in Fig. 9 for $P=0.5$ mT, and a H_2 percentage increased to 28% ($H_2/Cl_2=8/20$ sccm) corresponding to the lower limit of the onset of anisotropic etching regime at this pressure. Series of $A-C$ samples was etched in a single-step etch for different etching times. The results reported in Fig. 9 correspond to the type-*A* sample etched for 4 and 9 min, and to the type-*B* sample etched for 7 min. Although not shown, similar results were obtained for the type-*C* sample. A similar sidewall profile is observed with a smooth and almost vertical upper part showing no lateral etching difference between the different materials, and a slightly underetched bottom part where lateral

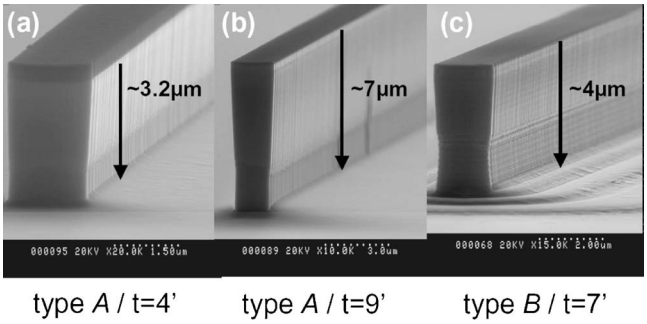

FIG. 9. SEM images of the [(a) and (b)] type-*A* and (c) type-*B* samples etched with $T=190$ °C, 0.5 mT, 800 W ICP power, −145 V dc bias, and $Cl_2/H_2=20/8$ sccm. The etching time is (a) 4 min., (b) 9 min., and (c) 7 min.. The samples are nonthermalized.

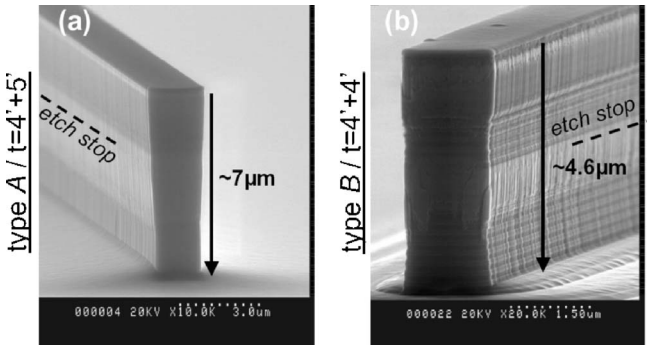

FIG. 10. SEM images of the [(a) and (b)] type-*A* and (c) type-*B* samples etched with $T=190\ ^\circ C$, 0.5 mT, 800 W ICP power, −145 V dc bias, and $Cl_2/H_2=20/8$ sccm in a two-step etch. The samples are nonthermalized.

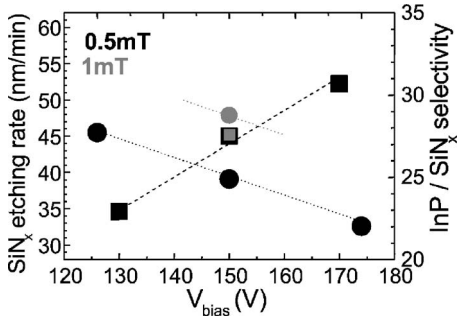

FIG. 12. Etching rate of the rf-PECVD SiN_x material (dots) and selectivity of SiN_x mask over InP (squares) measured for 800 W ICP power, $Cl_2/H_2=20/8$ sccm, and working pressures $P=0.5$ mT (black color) and $P=1$ mT (gray color). The dc bias is varied between −130 and −170 V for $P=0.5$ mT. The electrode temperature was set to 150 °C and the samples are nonthermalized.

etching difference between the InP and the quaternary or ternary layers is clearly apparent. This single-step etching behavior is independent of etching time and depth, and almost independent of the etched material as deduced from Fig. 9. But this etching mechanism is very sensitive to the sidewall conditions, as reported in Figs. 10(a) and 10(b) showing the etching profiles obtained for samples first etched for a few minutes, and then introduced again in the reactor to complete the etching (two-step etch).

A slight increase in the H_2 percentage in the 35%–45% range is sufficient to obtain reproducible, very smooth, and nearly vertical sidewalls for the $A-C$ samples, as illustrated in Fig. 11. It is worth mentioning that, in contrast with the Cl_2-Ar-H_2 etching optimization,[2] a high anisotropy without any notches at the ridge sidewalls was obtained here, despite the significant difference between the planar etching rates of the InP and InGa(Al)As materials. Etching rates of 1000, 340, and 380 nm/min were indeed measured for InP, InGaAlAs, and InGaAs, respectively, with $H_2/Cl_2=12/16$ sccm.

The samples in Fig. 11 were etched at an electrode temperature of 190 °C for comparison purposes with thermalized samples. However, the same etching profile and the same etching rate were obtained for an electrode temperature varied from 190 to 100 °C, while for the thermalized samples an electrode temperature higher than 150 °C is definitely required to maintain smooth etching. This observation confirms that the nonthermalized samples could be considered as thermally decoupled from the electrode.

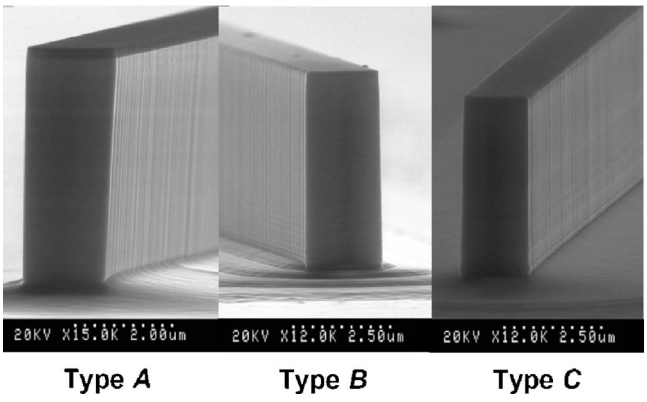

FIG. 11. SEM images of type-*A*, -*B*, and -*C* samples etched with $T=190\ ^\circ C$, 0.5 mT, 800 W ICP power, −145 V dc bias, and a total flow rate of 28 sccm. Samples are nonthermalized. The H_2 percentage is set in the 35%–45% range and the etch depth is ~5 μm.

Anisotropic ridge profiles with smooth sidewalls could be obtained for pressure values up to 1 mT by proper optimization of the H_2 concentration. Increasing the pressure further led to sidewall roughening and more isotropic etching.

An important outcome of the Cl_2-H_2 chemistry is the high etching selectivity over the SiN_x rf plasma-enhanced chemical-vapor deposition (rf-PECVD) dielectric mask. It was measured using a stylus profilometer on InP samples having a surface of $\sim 12\times 12\ mm^2$ and patterned with 20-μm-wide SiN_x mask stripes. Results are reported in Fig. 12. The SiN_x etching rate did not significantly change with pressure in the 0.5–1 mT pressure range, and was estimated to be ~40 nm/min for a dc bias of −145 V, corresponding to selectivity values as high as 24:1 and 29:1 for $P=0.5$ mT and $P=1$ mT, respectively. The etching selectivity can be influenced by the nature of the SiN_x material and by the loading effect that may reduce the InP etching rate for larger surface samples. However, our measured values are significantly higher than the typical values of ~13:1–17:1 usually reported in the literature[14,20] for dielectric masks. This higher selectivity is likely due to the reduced physical component in the Cl_2-H_2 mixture with no additive gas.

B. Modulator waveguide heterostructure etching

The optimized etching process at a pressure of 0.5 mT was finally used to etch a deep (>5 μm) ridge electroabsorption modulator structure, consisting of ten strained InGaAlAs quantum well active layers ($\lambda_g=1.48$ μm) and including a tapered region at one waveguide end. A highly anisotropic profile with smooth and nearly vertical sidewalls was obtained, as reported in Figs. 13(a) and 13(b). Moreover, the etching process did not affect the optical quality of the quantum wells (QWs), as evidenced from microphotoluminescence measurements performed before the epitaxial regrowth and reported in Fig. 13(c).

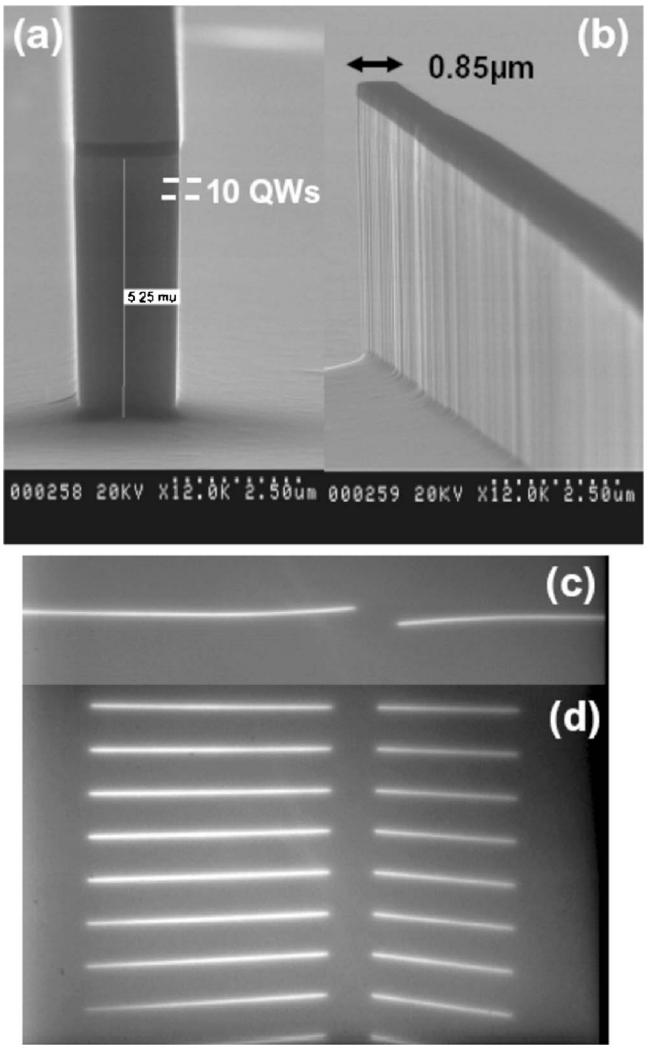

FIG. 13. [(a) and (b)] SEM profile of the electroabsorption modulator heterostructure etched with 800 W ICP power, −145 V dc bias, 0.5 mT, and $Cl_2/H_2=18/10$ sccm. The cathode temperature was set to 150 °C. The etch depth is 5.2 μm. The taper end is shown in (b). [(c) and (d)] Microphotoluminescence cartography of the deeply etched heterostucture, showing the good photoluminescence efficiency of the QWs after the etching process. The stripe width varies from 1.6 to 0.85 μm at the end of the taper region in (c), and is constant and equal to 0.85 μm in (d).

IV. CONCLUSION

We have studied the Cl_2/H_2 chemistry with no additive gas (CH_4, Ar, or N_2) to etch deep (>5 μm) InGa(Al)As/InP heterostructures with smooth and vertical sidewalls. We evidenced that the carrier material has a strong impact on the process optimization. We showed that the Cl_2/H_2 ratio is the main process parameter controlling the etching mechanism. This ratio should be adapted in a similar way for both bulk InP layers and InGa(Al)AsP/InP heterostructures to obtain vertical sidewalls, despite the strong planar etching rate difference between these materials. The process was optimized for nonthermalized InP wafers, in order to avoid the use of thermal grease that could be critical for subsequent technological steps. InP etching rates of 900–1300 nm/min and selectivities over SiN_x mask as high as 1:24–1:29 were obtained in the 0.5–1 mT pressure range at a high ICP power of 800 W. This process is well adapted to the realization of buried high-speed electroabsorption modulators with planar selective epitaxial regrowth, and could be used for the fabrication of highly confined deep ridge waveguides.

ACKNOWLEDGMENT

The authors thank I. Sagnes from Laboratoire de Photonique et de Nanostructures for providing the InP/InGaAs test heterostructure.

[1]S. Park, S.-S. Kim, L. Wang, and S.-T. Ho, IEEE J. Quantum Electron. **41**, 351 (2005).
[2]S. L. Rommel *et al.*, J. Vac. Sci. Technol. B **20**, 1327, (2002).
[3]A. Paraskevopoulos, D. Franke, P. Harde, S. Gouraud, M. Le Pallec, F. Lelarge, and J. Decobert, Proceedings of the 16th Indium Phosphide and Related Materials Conference, Kagoshima, Japan, 31 May-4 June 2004, Paper No, TuB-3-4, p. 122.
[4]R. van der Heijden *et al.*, Proceedings of the 17th Indium Phosphide and Related Materials Conference, Glasgow, Scotland, 8–12 May 2005, IEEE Catalog No. 05CH37633C.
[5]P. Strasser, R. Wüest, F. Robin, D. Erni, and H. Jäckel, Proceedings of the 16th Indium Phosphide and Related Materials Conference, Kagoshima, Japan, 31 May–4 June 2004, p. 175.
[6]C. F. Carlström, R. van der Heijden, F. Karouta, E. van der Drift, R. W. van der Heijden, H. W. M. Salemink, and E. van der Drift, J. Vac. Sci. Technol. B **24**, L6 (2006).
[7]C. Constantine, C. Barrat, S. J. Pearton, F. Ren, J. R. Lothian, W. S. Hobson, A. Katz, L. W. Yang, and P. C. Chao, Electron. Lett. **29**, 984 (1993).
[8]F. Karouta, E. J. Geluk, R. W. van der Heijden, A. Y. Silov, T. Eijkemans, J. J. G. M. van der Tol, M. K. Smit, and H. W. M. Salemink, Proceedings of the 16th Indium Phosphide and Related Materials Conference, Kagoshima, Japan, 31 May–4 June 2004, p. 322.
[9]S. Dupont, A. Beaurain, P. Miska, M. Zegaoui, J.-P. Vilcot, H. W. Li, M. Constant, D. Decoster, and J. Chazelas, Electron. Lett. **40**, 865 (2004).
[10]C. Constantine, C. Barrat, S. J. Pearton, F. Ren, and R. J. Lothian, Appl. Phys. Lett. **61**, 2899 (1992).
[11]S. Myakuni, R. Hattori, K. Sato, H. Takano, and O. Ishihara, J. Appl. Phys. **78**, 5734 (1995).
[12]J. Lin, A. Leven, N. G. Weiman, Y. Yang, R. F. Kopf, R. Reyes, Y. K. Chen, and F.-S. Choa, J. Vac. Sci. Technol. B **22**, 510 (2004).
[13]P. Strasser, R. Wüest, F. Robin, K. Rauscher, B. Wild, D. Erni, and H. Jäckel, Proceedings of the 17th Indium Phosphide and Related Materials Conference, Glasgow, Scotland, 8–12 May 2005, IEEE Catalog No. 05CH37633C.
[14]R. van der Heijden *et al.*, Proc. SPIE **5450**, 523 (2004).
[15]C. Youtsey and A. Adesisa, in *Handbook of Advanced Plasma Processing Techniques*, edited by R. J. Shul and S. J. Pearton (Springer, Berlin, 2000), Chap. 11, p. 466.
[16]A. Matsutani, H. Ohtsuki, S. Muta, F. Koyama, and K. Iga, Jpn. J. Appl. Phys., Part 1 **40**, 1528 (2001).
[17]A. Matsutani, H. Ohtsuki, F. Koyama, and K. Iga, Jpn. J. Appl. Phys., Part 1 **41**, 3147 (2002).
[18]N. St. J. Braithwaite, J. P. Booth, and G. Cunge, Plasma Sources Sci. Technol. **5**, 677 (1996).
[19]J. W. Lee, J. Hong, and S. J. Pearton, Appl. Phys. Lett. **68**, 847 (1996).
[20]C.-Z. Sun, J.-B. Zhou, B. Xiong, J. Wang, and Y. Luo, Chin. Phys. Lett. **20**, 1312 (2003).